

Ultra-flat and broad optical frequency combs generation based on novel dispersion-flattened double-slot microring resonator

Yuanwu Wang^{1,2} · Minming Zhang^{1,2} · Lulu Lu^{1,2} · Meifeng Li^{1,2} · Jinghao Wang^{1,2} · Feiya Zhou^{1,2} · Jing Dai^{1,2} · Lei Deng^{1,2} · Deming Liu^{1,2}

Received: 1 September 2015 / Accepted: 17 November 2015 / Published online: 20 January 2016
© Springer-Verlag Berlin Heidelberg 2016

Abstract In this paper, a novel double-slot microring resonator is proposed to produce flat dispersion of 0–3.8 ps/(nm km) over 1150 nm wavelength range. Moreover, the dispersion tailoring with different structural parameters of the proposed microring resonator is analyzed and simulated. The simulation results show that the dispersion fluctuation can be tailored by the height of the central and bottom As_2S_3 layer, and the slope can be adjusted by the waveguide width and lower SiO_2 slot thickness. Furthermore, by means of the Lugiato–Lefever equation, an ultra-flat and broad optical frequency comb with 7-dB bandwidth of 1155 nm (1855–3010 nm) is obtained based on such dispersion-optimized resonator. The proposed double-slot microring resonator shows potential application in both telecommunication and mid-infrared research domain.

1 Introduction

The optical frequency combs based on microresonators [1–6] which have attractive features such as wide spectral range, high repetition rate and integration have gained considerable attention in astronomy, spectroscopy, arbitrary waveform generator, optical clocks and telecommunication [6, 7]. However, for a high-quality optical frequency comb, the broader coverage in wavelength and less variation in

amplitude are of great importance. Microresonator-based frequency combs are generated owing to cascaded four-wave mixing effect, which is seriously influenced by the dispersion and nonlinearity [8]. Thus, the dispersion tailoring and high nonlinearity of microresonator are vital for the optical frequency comb generation. In the dispersion aspect, the appropriate dispersion profile could produce desirable phase matching of the four-wave mixing responsible for the comb generation and efficiently regulate the ultimate spectral coverage and flatness of the combs [9, 10].

For a broader and flatter frequency combs generation, the key factor is to acquire a lower and flatter dispersion curve over a wide wavelength range of the microresonator. Recently, the waveguide structures with a strip [11], single-slot [12–15] and double-slot waveguide [16, 17] have been proposed to tailor the dispersion profile. Due to the unique capability of dispersion engineering, the single-slot waveguide was explored in a microresonator for a flattened dispersion [18, 19]. Zhang et al. reported that dispersion variation of the single-slot microring resonator was fluctuated from 0 to 17 ps/(nm km) [18]. More recently, Bao and Zhang found the dispersion varied between 0 and 7.2 ps/(nm km) over 718-nm bandwidth in the same waveguide structure, corresponding to the optical frequency combs spectrum with 10-dB bandwidth of 630 nm [19].

In this paper, the ultra-flat and broad optical frequency combs with a 7-dB power variation of comb lines from 1855 to 3010 nm wavelength are successfully achieved by simulation on the basis of our original microring resonator. The proposed resonator is formed of arsenic tri-sulfide (As_2S_3) double-slot waveguides and shows an ultra-flat and low dispersion of 0–3.8 ps/(nm km) over a 1150 nm wavelength range. Furthermore, the impact of different

✉ Minming Zhang
mmz@hust.edu.cn

¹ School of Optical and Electronic Information, Huazhong University of Science and Technology, Wuhan 430074, China

² National Engineering Laboratory for Next Generation Internet Access System, Huazhong University of Science and Technology, Wuhan 430074, China

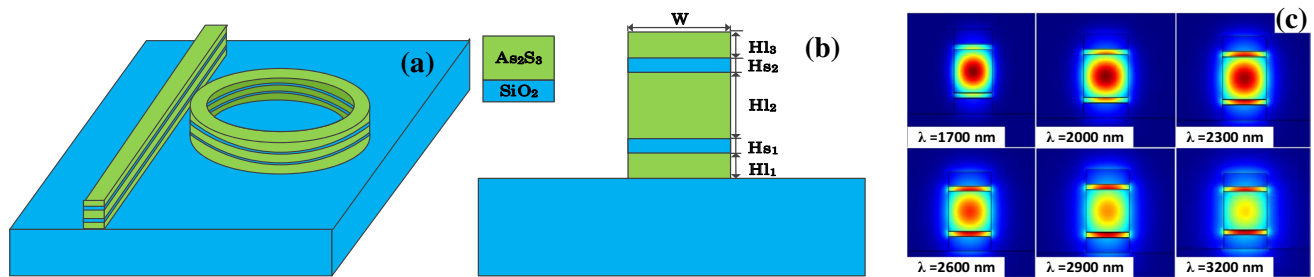


Fig. 1 **a** Double-slot waveguide-based microring resonator. **b** Cross section and material of double-slot microring waveguide. **c** The mode evolution of quasi-TM mode (*vertical direction*) at different wavelengths, respectively

structural parameters of microring waveguide on the dispersion profile is analyzed.

2 Waveguide structure and dispersion property

Compared with the type of single-slot structure, double-slot waveguide has more dimensions to design; meanwhile, ultra-broadband, flat and low-dispersion profiles can be achieved and shaped by tailoring structural parameters [16, 17]. Here, the double-slot waveguide is combined with microring resonator in the first time for the flatter and broader optical frequency comb generation, to the best of our knowledge.

Figure 1a shows the basic structure of the designed double-slot waveguide-based microring resonator. The bending radius (R) of the microring resonator is $117\ \mu\text{m}$, corresponding to the free spectral range (FSR) of 200 GHz. The pump light is launched from a straight waveguide and coupled into the microring resonator. As shown in Fig. 1b, the waveguide has two horizontal SiO_2 slots which are surrounded by three As_2S_3 layers. Additionally, the substrate of the waveguide is $4\text{-}\mu\text{m}$ -thick SiO_2 , and the upper cladding is air. Moreover, W , HL_1 , Hs_1 , HL_2 , Hs_2 and HL_3 represent the waveguide width, bottom As_2S_3 height, lower SiO_2 slot thickness, central As_2S_3 height, upper SiO_2 slot thickness and upper As_2S_3 height, respectively.

Figure 1c shows the mode evolution of quasi-TM mode (*vertical direction*) at different wavelengths. The principle of dispersion tailoring of the double-slot waveguide can be explained as follows: The anticrossing effect that the guided mode transits from a strip mode at short wavelength to a slot-like mode at long wavelength could lead to the flattened dispersion and finally produce a slightly negative waveguide dispersion for balancing the convex dispersion in strip waveguides without a slot structure [17].

The dispersion profiles $D(\lambda)$ are performed by using the finite element method. The dispersion of quasi-TM mode (*vertically polarized*) is calculated by the second derivative of the effective index (n_{eff}) with respect to the wavelength (λ). It is defined as follows:

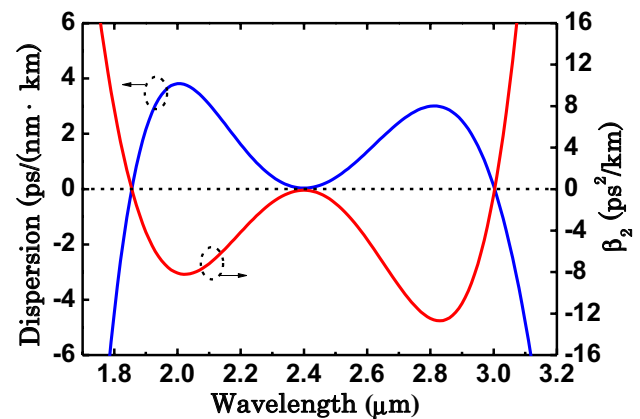


Fig. 2 Dispersion and second-order dispersion coefficient profile of the optimum waveguide structure I

$$D = -(\lambda/c) \cdot \left(\partial^2 n_{\text{eff}} / \partial \lambda^2 \right), \quad (1)$$

where c is the speed of light in vacuum. In the calculation, the wavelength step and effective index precision are 10 nm and 16 float digits, respectively. In this work, material dispersion of As_2S_3 and SiO_2 is also taken into account [20, 21].

The structure parameters of the waveguide including W , HL_1 , Hs_1 , HL_2 , Hs_2 and HL_3 can be properly tuned for tailoring the dispersion when needed. As seen from Fig. 2, by optimizing structure parameters (structure I) as $W = 933\ \text{nm}$, $HL_1 = 330\ \text{nm}$, $Hs_1 = 114\ \text{nm}$, $HL_2 = 960\ \text{nm}$, $Hs_2 = 112\ \text{nm}$, $HL_3 = 328\ \text{nm}$ and $R = 117\ \mu\text{m}$, a saddle-shaped dispersion profile with two zero-dispersion wavelengths (ZDWs) is achieved. The ultra-flat and low-dispersion value D varies in $0\text{--}3.8\ \text{ps}/(\text{nm}\ \text{km})$ from 1855 to 3005 nm over a 1150-nm bandwidth. Correspondingly, the second-order dispersion coefficient β_2 ($\beta_2 = -\lambda^2 D / 2\pi c$) changes within $0 \sim -12.6\ \text{ps}^2/\text{km}$. Compared with the single-slot waveguide-based microring resonator in Reference [18] which showed D varies in $0\text{--}17\ \text{ps}/(\text{nm}\ \text{km})$, accordingly β_2 varies from 0 to $16\ \text{ps}^2/\text{km}$, the dispersion profile of the proposed method is lower and flatter (see above).

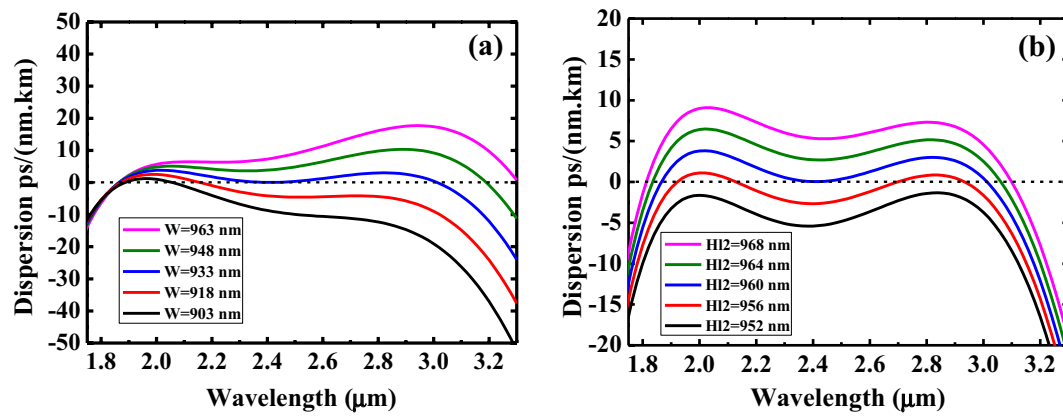


Fig. 3 Dispersion profiles with the variation of **a** waveguide width W , **b** central As_2S_3 height H_{l2} , respectively, in the structure I

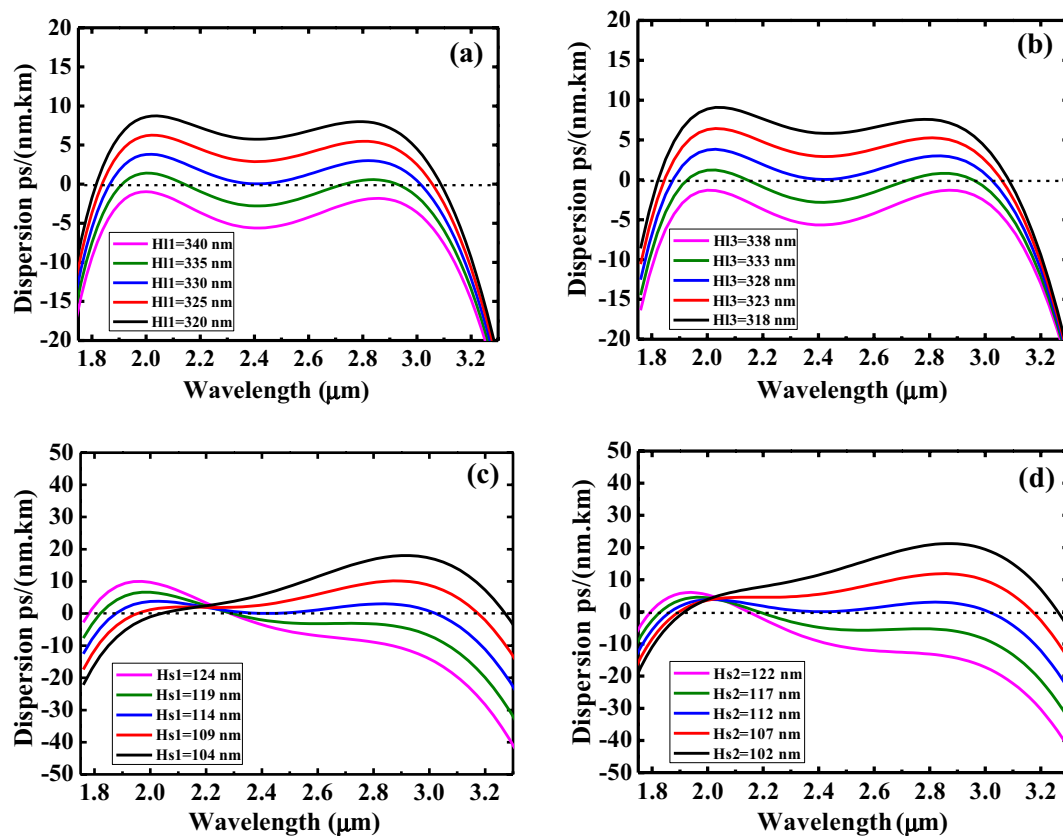


Fig. 4 Dispersion profiles with the variation of **a** bottom As_2S_3 height H_{l1} , **b** upper As_2S_3 height H_{l3} , **c** lower SiO_2 slot thickness H_{s1} , **d** upper SiO_2 slot thickness H_{s2} , respectively, in the structure I

3 Principle of dispersion tailoring

The dispersion can be tailored by tuning the structural parameters of double-slot microring resonator waveguide. So the effect of each structural parameter on the dispersion properties is investigated by changing it around the optimum value while the other parameters are kept the

same. The dispersion profiles of the waveguide as shown in Figs. 3 and 4 are effectively tailored by properly tuning the parameters W , H_{l2} , H_{l1} and H_{s1} .

As shown in Fig. 3a, changing the waveguide width W could adjust the flatness of dispersion profile while other structural parameters are constant. Dispersion values in long wavelength range are more sensitive to fluctuations of W , and both the

shape and slope of dispersion profile are efficiently changed. Meanwhile, the sign of third-order dispersion (TOD) could be effectively regulated with changing the W . During optimizing the dispersion profile, the change of the central As_2S_3 height HI_2 could flexibly adjust the fluctuation of the entire dispersion curves. As shown in Fig. 3b, when the HI_2 decreases from 968 to 952 nm with other parameters unchanged (structure I), the dispersion moves up from anomalous dispersion to normal dispersion regime with almost the same shape and slope, and the dispersion value change is 0.7 ps/(nm km) per nm. The number of ZDWs firstly changes from 2 to 4 and then decreases to 0 as the HI_2 decreases from 968 to 952 nm. The decrease in HI_2 promotes mode transition from strip mode to slot mode. Obviously, negative waveguide dispersion by this transition moves down the dispersion curves.

There is a similar trend in both situations when the bottom As_2S_3 height HI_1 or upper As_2S_3 height HI_3 is decreased and the central As_2S_3 height HI_2 is increased. As shown in Fig. 4a, b, the reduction in HI_1 and HI_3 causes the moving of the dispersion profile from normal to anomalous dispersion regime with a dispersion value change of 0.5 ps/(nm km) per nm. Moreover, the number of ZDWs firstly changes from 2 to 4 and then decreases to 0 with the increase in HI_1 and HI_3 . Furthermore, the flatness of total dispersion profiles can be improved. The sign of third-order dispersion (TOD) dispersion slope can be finely controlled by properly tuning the lower SiO_2 slot thickness Hs_1 and upper SiO_2 slot thickness Hs_2 as shown in Fig. 4c, d, respectively. The dispersion curves imply that the long wavelength part goes down while the short wavelength part almost remains consistent with Hs_1 increasing from 104 to 124 nm, and the dispersion curves nearly rotate at 2230 nm. Meanwhile, the dispersion curves have the same trend when Hs_2 increases from 102 to 122 nm, and the dispersion curves nearly rotate at 2020 nm in Fig. 4d. Therefore, the slope can be flexibly modified by tailoring the lower and upper slot thickness of waveguides.

As shown in Figs. 3 and 4, the optimal dispersion profile could be achieved when the structural parameters changed in double-slot microring resonator waveguides; meanwhile, the dispersion deviation is only ± 20 ps/(nm km). However, compared with the single- or double-slot silicon waveguide [12, 16, 17] with ± 200 ps/(nm km) dispersion deviation in the same variations of structural parameters, this double-slot arsenic tri-sulfide waveguide has less sensitivity to variations of the structural parameters and fabrication errors.

4 Flat optical frequency combs generation in double-slot microring resonator

From Reference [22], it can be predicted that the optical frequency comb is more easily generated when the dispersion is in anomalous area. Furthermore, the comb performance can

be considerably influenced by the value of β_2 and the bandwidth (BW) between two zero-dispersion points (ZDPs) [19, 23]. Generally speaking, the lower the β_2 , the flatter the comb generation, and the broader the BW between two ZDPs, the broader the comb bandwidth generation. Consequently, the dispersion profile of structure I in the simulation is adopted for flatter and broader frequency combs generation.

In order to simulate flatter and broader comb generation based on the optimized dispersion profile of the structure I, the Lugiato–Lefever equation [24–26] is utilized as follows:

$$t_R \cdot \frac{\partial E(t, \tau)}{\partial t} = \left[-\alpha - i\delta_0 + iL \sum_{k \geq 2} \frac{\beta_k}{k!} \left(i \frac{\partial}{\partial \tau} \right)^k + i\gamma L |E|^2 \right] E + \sqrt{\theta} E_{in}, \quad (2)$$

where t_R is the round-trip time and α describes the total cavity losses per round trip including the linear absorption inside the resonator and the power coupling coefficient θ . δ_0 means the cavity detuning, and L stands for cavity length. Other resonator parameters include the k th dispersion coefficient β_k ($\beta_k = d^k \beta / d\omega_k$) and the nonlinear coefficient γ ($\gamma = n_2 \omega_0 / (c A_{eff})$, n_2 the nonlinear refractive index, A_{eff} the effective modal area of the resonator mode). $E(t, \tau)$ and E_{in} are the intra-cavity field and input field (pump power $P_{in} = |E_{in}|^2$), respectively, where t and τ are the slow and fast times.

In our simulation, parameters are taken from the double-slot microring resonator of structure I, with the FSR = 200 GHz, under $R = 117 \mu\text{m}$, $L = 735 \mu\text{m}$ and $P_{in} = 100$ mW. Here, α and θ are equal to 0.009 [27], the calculated cavity Q factor is approximate to 3×10^5 , and calculated γ is about 8000 (1/W/km). The pump wavelength is close to 2.33 μm . Through turning the detuning as 0.086, the ultra-flat optical frequency combs with a 7-dB power variation of comb lines from 1855 to 3010 nm wavelength over 1155-nm bandwidth are gained and shown in Fig. 5. In general, the flatness or bandwidth of comb spectrum is measured in a 20-dB power variation with 1110-nm bandwidth [18] or 10-dB power variation with 630-nm bandwidth [19]. Meanwhile, compared with References [18, 19], the broader bandwidth of the output comb spectrum is obtained with the smaller power variation in our study. Specially, we note that there are two strong narrow-band peaks in the output, which are the dispersive waves and around the second-order dispersion coefficient to zero, as mentioned in Reference [26].

As shown in Reference [28], the dispersion-induced change of the FSR could be minimized due to the low and flat cavity dispersion profile, which helps to generate a nearly equidistant frequency comb. Specially, in our design, the FSR standard deviation is as low as 0.052 GHz, providing potential

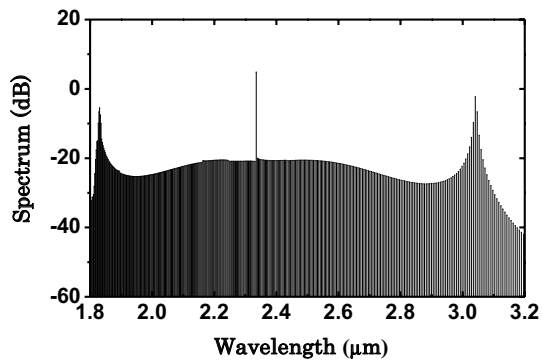


Fig. 5 Output frequency comb spectra of structure I with the given parameters

for optical carriers of large capacity communication transmission. In addition, the optical frequency combs are located in mid-infrared range, which not only add tremendous value to existing applications including the optical communication in 2- μm waveband and precision spectroscopy of molecules, but also have a strong impact on emerging or unknown fields throughout many areas of research [29–31].

5 Conclusion

In conclusion, by tailoring the structural parameters of the proposed double-slot microring resonator based on an As_2S_3 waveguide, the ultra-flat and low dispersion over a wide bandwidth range is provided. The influence of the structure parameters on the dispersion curves is studied. Moreover, the optimized dispersion profile is of great importance for improving the performance of cascaded four-wave mixing and frequency comb generation in microresonator. Finally, an ultra-flat, broad and nearly equidistant frequency comb based on the optimized dispersion profile is generated with the Lugiato–Lefever equation in simulation, which is also potentially useful for both telecommunication and mid-infrared applications.

Acknowledgments This work is supported by the National High Technology Research and Development Program of China (863 Program, Grant No. 2015AA015504), the Major Project of Science and Technology Innovation Program of Hubei Province of China (Grant No. 2014AAA006) and National Natural Science Foundation of China (Grant No. 61107051).

References

- P. Del’Haye, A. Schliesser, O. Arcizet, T. Wilken, R. Holzwarth, T.J. Kippenberg, Optical frequency comb generation from a monolithic microresonator. *Nature* **450**, 1214–1217 (2007)
- A.A. Savchenkov, A.B. Matsko, V.S. Ilchenko, I. Solomatine, D. Seidel, L. Maleki, Tunable optical frequency comb with a crystalline whispering gallery mode resonator. *Phys. Rev. Lett.* **101**, 093902–093905 (2008)
- Y. Okawachi, A.L. Gaeta, M. Lipson, Breakthroughs in nonlinear silicon photonics 2011. *IEEE Photon. J.* **4**, 601–606 (2012)
- J.S. Levy, A. Gondarenko, M.A. Foster, A.C. Turner-Foster, A.L. Gaeta, M. Lipson, Cmos-compatible multiple-wavelength oscillator for on-chip optical interconnects. *Nat. Photon.* **4**, 37–40 (2010)
- L. Razzari, D. Duchesne, M. Ferrera, R. Morandotti, S. Chu, B.E. Little, D.J. Moss, Cmos-compatible integrated optical hyper-parametric oscillator. *Nat. Photon.* **4**, 41–45 (2010)
- T.J. Kippenberg, R. Holzwarth, S.A. Diddams, Microresonator-based optical frequency combs. *Science* **332**, 555–559 (2011)
- N.R. Newbury, Searching for applications with a fine-tooth comb. *Nat. Photon.* **5**, 186–188 (2011)
- T. Herr, K. Hartinger, J. Riemensberger, C. Wang, E. Gavartin, R. Holzwarth, M.L. Gorodetsky, T.J. Kippenberg, Universal formation dynamics and noise of Kerr-frequency combs in microresonators. *Nat. Photon.* **6**, 480–487 (2012)
- P. Del’Haye, T. Herr, E. Gavartin, M.L. Gorodetsky, R. Holzwarth, T.J. Kippenberg, Octave spanning tunable frequency comb from a microresonator. *Phys. Rev. Lett.* **107**, 063901–063905 (2011)
- Y. Okawachi, K. Saha, J.S. Levy, Y.H. Wen, M. Lipson, A.L. Gaeta, Octave-spanning frequency comb generation in silicon nitride chip. *Opt. Lett.* **36**, 3398–3400 (2011)
- Y. Yue, L. Zhang, H. Huang, R.G. Beausoleil, A.E. Willner, Silicon-on-nitride waveguide with ultralow dispersion over an octave-spanning mid-infrared wavelength range. *IEEE Photon. J.* **4**, 126–132 (2012)
- L. Zhang, Y. Yue, R.G. Beausoleil, A.E. Willner, Flattened dispersion in silicon slot waveguides. *Opt. Express* **18**, 20529–20534 (2010)
- A.E. Willner, L. Zhang, Y. Yue, “Tailoring of dispersion and nonlinear properties of integrated silicon waveguides for signal processing applications”. *Semicond. Sci. Technol.* **26**, 014044–014051 (2011)
- S.F. Wang, J.G. Hu, H.R. Guo, X.L. Zeng, Optical Cherenkov radiation in an As_2S_3 slot waveguide with four zero-dispersion wavelengths. *Opt. Express* **21**, 3067–3072 (2013)
- Z. Jafari, F. Emami, Strip/slot hybrid arsenic tri-sulfide waveguide with ultra-flat and low dispersion profile over an ultra-wide bandwidth. *Opt. Lett.* **38**, 3082–3085 (2013)
- C.J. Bao, Y. Yan, L. Zhang, Y. Yue, A.E. Willner, “Tailoring of Low Chromatic Dispersion over a Broadband in Silicon Waveguides using a Double-Slot Design,” in Conference on Lasers and Electro-Optics (CLEO) 2013, paper JTu4A.53
- M. Zhu, H.J. Liu, X.F. Li, N. Huang, Q.B. Sun, J. Wen, Z.L. Wang, Ultra broadband flat dispersion tailoring of dual slot silicon waveguides. *Opt. Express* **20**, 15899–15907 (2012)
- L. Zhang, C.Y. Bao, V. Singh, J.W. Mu, C.X. Yang, A.M. Agarwal, L.C. Kimerling, J. Michel, “Generation of two-cycle pulses and octave-spanning frequency combs in a dispersion-flattened micro-resonator”. *Opt. Lett.* **38**, 5122–5125 (2013)
- C.J. Bao, L. Zhang, Y. Yan, H. Huang, G.D. Xie, A.M. Agarwal, L.C. Kimerling, J. Michel, A.E. Willner, “Tailoring of a Broader and Flatter Frequency Comb using a Microring Resonator with a Low-Index Slot,” in Conference on Lasers and Electro-Optics (CLEO) 2014, paper SM1M.5
- W.S. Rodney, I.H. Malitson, T.A. King, Refractive index of arsenic trisulfide. *J. Opt. Soc. Am.* **48**, 633–636 (1958)
- M.J. Weber, *Handbook of Optical Material* (CRC Press, Boca Raton, 2002)
- C. Godey, I. Balakireva, A. Coillet, Y. Chembo, Stability analysis of the spatiotemporal Lugiato–Lefever model for Kerr optical frequency combs in the anomalous and normal dispersion regimes. *Phys. Rev. A* **89**, 063814–063821 (2014)

23. S. Coen, M. Erkintalo, Universal scaling laws of Kerr frequency combs. *Opt. Lett.* **38**, 1790–1792 (2013)
24. L.A. Lugiato, R. Lefever, Spatial dissipative structure in passive optical systems. *Phys. Rev. Lett.* **58**, 2209–2211 (1987)
25. S. Coen, H.G. Randle, T. Sylvestre, M. Erkintalo, Modeling of octave-spanning Kerr frequency combs using a generalized mean-field Lugiato–Lefever model. *Opt. Lett.* **38**, 37–39 (2013)
26. M.R.E. Lamont, Y. Okawachi, A.L. Gaeta, Route to stabilized ultrabroadband microresonator-based frequency combs. *Opt. Lett.* **38**, 3478–3481 (2013)
27. B.J. Eggleton, B. Luther-Davies, K. Richardson, Chalcogenide photonics. *Nat. Photon.* **5**, 141–148 (2011)
28. L. Zhang, Y. Yue, R.G. Beausoleil, A.E. Willner, Analysis and engineering of chromatic dispersion in silicon waveguide bends and ring resonators. *Opt. Express* **19**, 8102–8107 (2011)
29. N. MacSuihbne, Z. Li, B. Baeuerle et al. “Wavelength division multiplexing at 2 μm ,” in European Conference and Exposition on Optical Communications (ECOC) 2012, paper Th.3.A.3
30. C.Y. Wang, T. Herr, P. Del’Haye, A. Schliesser, J. Hofer, R. Holzwarth, T.W. Hansch, N. Picque, T.J. Kippenberg, Mid-infrared optical frequency combs at 2.5 μm based on crystalline microresonators. *Nat. Commun.* **4**, 1435–1440 (2013)
31. A. Schliesser, N. Picqué, T.W. Hänsch, Mid-infrared frequency combs. *Nat. Photon.* **6**, 440–446 (2012)